Available online at www.sciencedirect.com
SCIENCE DIRECT®
Ocean Modelling 6 (2004) 245–263
Ocean Modelling
www.elsevier.com/locate/omodol

Tidally driven mixing in a numerical model of the ocean general circulation

Harper L. Simmons [a,b,*], Steven R. Jayne [c], Louis C. St. Laurent [d], Andrew J. Weaver [e]

[a] International Arctic Research Center, University of Alaska Fairbanks, Fairbanks, AK 99775-7340, USA
[b] Geophysical Fluid Dynamics Laboratory, P.O. Box 308, Princeton, NJ 08542-0308, USA
[c] Physical Oceanography Department, Woods Hole Oceanographic Institution, Woods Hole, MA 02543, USA
[d] Department of Oceanography, Florida State University, Tallahassee, FL 32306-4320, USA
[e] School of Earth and Ocean Sciences, University of Victoria, Vic., BC, Canada V8W 3P6

Received 7 June 2002; received in revised form 30 January 2003; accepted 30 January 2003

Abstract

Astronomical data reveals that approximately 3.5 terawatts (TW) of tidal energy is dissipated in the ocean. Tidal models and satellite altimetry suggest that 1 TW of this energy is converted from the barotropic to internal tides in the deep ocean, predominantly around regions of rough topography such as mid-ocean ridges. A global tidal model is used to compute turbulent energy levels associated with the dissipation of internal tides, and the diapycnal mixing supported by this energy flux is computed using a simple parameterization.

The mixing parameterization has been incorporated into a coarse resolution numerical model of the global ocean. This parameterization offers an energetically consistent and practical means of improving the representation of ocean mixing processes in climate models. Novel features of this implementation are that the model explicitly accounts for the tidal energy source for mixing, and that the mixing evolves both spatially and temporally with the model state. At equilibrium, the globally averaged diffusivity profile ranges from 0.3 $cm^2\,s^{-1}$ at thermocline depths to 7.7 $cm^2\,s^{-1}$ in the abyss with a depth average of 0.9 $cm^2\,s^{-1}$, in close agreement with inferences from global balances. Water properties are strongly influenced by the combination of weak mixing in the main thermocline and enhanced mixing in the deep ocean. Climatological comparisons show that the parameterized mixing scheme results in a substantial reduction

* Corresponding author. Address: International Arctic Research Center, University of Alaska Fairbanks, Fairbanks, AK 99775, USA.
E-mail address: hsimmons@iarc.uaf.edu (H.L. Simmons).

1463-5003/$ - see front matter
doi:10.1016/S1463-5003(03)00011-8

of temperature/salinity bias relative to model solutions with either a uniform vertical diffusivity of 0.9 $cm^2 s^{-1}$ or a horizontally uniform bottom-intensified arctangent mixing profile. This suggests that spatially varying bottom intensified mixing is an essential component of the balances required for the maintenance of the ocean's abyssal stratification.

1. Introduction

Modeling studies have shown that oceanic heat transports are extremely sensitive to variations in the diffusivity (Bryan, 1987; Marotzke, 1997; Zhang et al., 1999). Variations in diffusivity have also been shown to have a large impact on the modeled uptake and storage of climatically important tracers such as carbon (Sokolov et al., 1998). Presently popular schemes for parameterizing mixing utilize fixed values of diapycnal diffusivity. These are usually assigned ad hoc, as a means of tuning the model's meridional transports of heat and mass. While this practice results in aligning modeled properties with the presently observed state of the ocean, the parameterized rate of mixing has no ability to evolve with a changing ocean. This is problematic, as understanding and predicting changes in the state of the ocean, and hence the climate system, is a primary goal of most modeling efforts. We require more physically based mixing parameterizations, which not only energetically constrain the mixing in the present oceanic system, but also allow mixing to evolve with a changing climate system.

Observed turbulent diffusivities in the ocean interior range from 0.1 $cm^2 s^{-1}$ in the thermocline (Ledwell et al., 1993, 1998) to greater than 10 $cm^2 s^{-1}$ in the deep ocean above regions of rough topography (Polzin et al., 1997; Ledwell et al., 2000). To sustain these turbulent diffusivities, there must be a constant supply of mechanical energy. The main source of this energy is the internal wave field of the ocean. Some internal wave energy is derived from the transmission of wind energy through the surface mixed layer (Alford, 2001; Watanabe and Hibiya, 2002). Tidal flow over seafloor topography acts as an additional source of internal waves in the deep ocean. Previously, the global distribution of energy flux into the internal tides has been examined using observations and tidal models (Egbert and Ray, 2000, 2001; Jayne and St. Laurent, 2001; Niwa and Hibiya, 2001). While a direct connection between wind forcing and interior mixing has not been established, observational studies have shown that mixing rates are enhanced in regions of internal tide generation (Kunze and Toole, 1997; Lueck and Mudge, 1997; Polzin et al., 1997; Ledwell et al., 2000; Lien and Gregg, 2001; Pinkel et al., 2001; Kunze et al., 2002; Moum et al., 2002).

There are several studies which are a logical antecedent to the present work. Huang (1999) has argued that ocean models must consider the energy available for mixing, and implemented a scheme in which a fixed energy dissipation profile was used to calculate diffusivity in an idealized sector model. Hasumi and Suginohara (1999) investigated the effects of enhancing vertical diffusivity over rough topography. They modified the mixing in the deep ocean by enhancing the vertical diffusivity in areas where the sub-grid scale roughness exceeded a specified threshold. They found that upwelling of deep and bottom waters was confined to areas where the vertical diffusivity was enhanced. Their experiments clearly point out the importance of the distribution of vertical mixing as a control on the abyssal circulation. Huang and Xiangze (2002) took a similar approach to Hasumi and Suginohara, but considered a regional model of the South Atlantic.

Gargett (1984) explored the dynamical connection between meridional transport and a stratification dependent mixing of the form $k_v \propto N^{-1}$. The consequences of this mixing scheme for a numerical ocean model were investigated by Cummins et al. (1990). An ad hoc arctangent diffusivity profile, weak in the thermocline and increasing with depth, has been used in many ocean models (Bryan and Lewis, 1979). This profile has been rationalized a postiori based both on more recent observations of enhanced mixing in the deep ocean and for its ability to improve water mass distributions in numerical models. Mixing schemes based on local energy arguments have also been implemented in ocean models (Pacanowski and Philander, 1981; Large et al., 1994). These schemes often have a vertical diffusivity related to Richardson number and generally employ some sort of background diffusivity profile which dominates the Richardson number dependent mixing through-out most of the ocean. Without the impractically high resolution capable of supporting an internal wave spectrum and cascade, these Richardson number based schemes cannot account for mixing supported by the baroclinic tides.

2. Inferences and observations of ocean mixing

One method of quantifying mixing in the ocean is through large scale balances of mass, heat and salt. Based on an assumed estimate of the upwelling, Munk (1966) inferred that Pacific intermediate and abyssal waters (i.e., water between 1000 and 4000 m) mix with an average diffusivity of 1 $cm^2\,s^{-1}$. Abyssal water mass conversions in the Brazil Basin have been studied using hydrography, current meter measurements, and control volume methods (Hogg et al., 1982; Morris et al., 2001). These studies suggest that O(l) $cm^2\,s^{-1}$ diffusivities are indeed influencing in the basin-averaged budgets of heat and mass. Deep diffusivity estimates in excess of O(l) $cm^2\,s^{-1}$ have been derived for many semi-enclosed basins (Whitehead and Worthington, 1982; Saunders, 1987; Barton and Hill, 1989; Roemmich et al., 1996; Ferron et al., 1998; Heywood et al., 2002).

Another perspective on mixing comes from the consideration of global energy balances. In order to maintain the observed density stratification against an assumed overturning rate, Munk and Wunsch (1998) calculated that 2 TW must be dissipated throughout the ocean, although this amount has been disputed by Webb and Suginohara (2001). Independent analysis of the tides using analytical methods, altimetry, and tidal modeling reveals that approximately 1 TW of energy is lost from the barotropic tides in the generation of internal tides (Egbert and Ray, 2000, 2001; Jayne and St. Laurent, 2001). This energy must ultimately be dissipated, presumably supporting diapycnal mixing. Additional energy required to maintain the inferred mixing is thought to be provided by the wind work on the ocean general circulation (Munk and Wunsch, 1998; Wunsch, 1998; Alford, 2001).

Direct measurements of mixing in the upper ocean and thermocline (but below the mixed layer) consistently reveal smaller diffusivities near 0.1 $cm^2\,s^{-1}$. Similar values are observed throughout the full ocean depth over smooth abyssal plains, and appear to represent a background level of turbulence supported by the internal wave continuum (Munk, 1981). Above rough topography, mixing rates are observed to be orders of magnitude above background levels (Polzin et al., 1997; Ledwell et al., 2000). In these locations, elevated diffusivities extend hundreds of meters above the ocean floor.

3. A parameterization of ocean mixing

Our goal is to introduce a new, more physically based, energetically constrained and consistent parameterization of mixing into an ocean general circulation model (OGCM). This parameterization is discussed more extensively in St. Laurent et al. (2002). Enhanced mixing levels are assumed to be supported by energy flux into the internal tides estimated from a model of the barotropic tides (Jayne and St. Laurent, 2001).

In the tidal modeling study of Jayne and St. Laurent (2001), a term for internal wave drag due to oscillating flow over topography of the form

$$D = \tfrac{1}{2} N_{\mathrm{b}} \kappa h^2 \boldsymbol{u}, \tag{1}$$

was added to the Laplace tidal equations. In (1), N_{b}, is the climatological buoyancy frequency along the seafloor, (κ, h) are the wavenumber and amplitude scales for the topographic roughness, and $\boldsymbol{u}$ is the barotropic tidal velocity predicted by the model. The drag term (1) has an adjustable parameter, κ, representing a characteristic topographic wavenumber responsible for the generation of internal waves. The parameter κ was set so that the modeled barotropic tides best matched observed tides in a least-squared sense.

Energy flux per unit area out of the barotropic tides was diagnosed from the wave drag (1) as

$$E(x, y) = \tfrac{1}{2} \rho_0 N_{\mathrm{b}} \kappa h^2 \langle \boldsymbol{u}^2 \rangle, \tag{2}$$

where ρ_0 is a reference density for seawater, and $\langle \boldsymbol{u}^2 \rangle$ is the temporal mean-square tidal velocity. It was found that 1.10 TW of energy was dissipated by the wave drag parameterization in the deep ocean (depths greater than 1000 m), in agreement with independent estimates (Egbert and Ray, 2000, 2001). It is important to emphasize that the parameter κ in (1) was tuned to fit observations of tidal sea-surface elevation, *not* the tidal dissipation rate. The Jayne and St. Laurent (2001) model provides the tidal energy estimates for our mixing parameterization.

To transform estimates of energy flux from (2) to a three-dimensional map of diapycnal mixing, it is important to consider the physics of internal tide generation. When a tidal flow encounters rough topography, a wavenumber spectrum of internal waves is generated. Some portion of this spectrum is dissipated locally, with the remaining portion radiating away to dissipate at large distances from the generation site (St. Laurent and Garrett, 2002). Physical arguments suggest that 60–90% of this baroclinic wave energy is contained in low-mode internal waves that are able to propagate large distances from the generation site. The remaining portion of the energy lost from the barotropic tide, denoted the "tidal dissipation efficiency" (q), dissipates as *locally enhanced* turbulent mixing. St. Laurent et al. (2002) assumed that $q = 1/3$ of the generated energy flux is dissipated locally, with the remaining $1 - q = 2/3$ radiating away as low mode internal waves. An assumed vertical structure $F(z)$ for the turbulent dissipation rate (ϵ), finally allows us to relate estimates from (2) to a profile of turbulent dissipation. Using the Osborn (1980) model of mixing efficiency to relate dissipation to diffusion, our parameterization is

$$k_v = k_0 + \frac{\Gamma \epsilon}{N^2} = k_0 + \frac{q \Gamma E(x, y) F(z)}{\rho N^2}, \tag{3}$$

where $F(z)$ is the vertical redistribution function, and q is the tidal dissipation efficiency. Here, Γ is the mixing efficiency, taken to be 0.2 (Osborn, 1980), and $E(x, y)$ is recomputed using (2) with $\boldsymbol{u}$

taken from the tidal model, but N_b and N from the ocean model. Thus both the energy flux and the diffusivity evolve as part of the model solution. We justify recomputing E using the evolving stratification on the grounds that the barotropic tidal velocity $\boldsymbol{u}$ is only weakly dependent on the stratification. The parameter k_0 is a weak background diffusivity added in to account for other non-local sources of mixing. This background mixing may account for dissipating low-mode internal tides, as well as other sources such as radiating near-inertial waves generated by winds over the surface mixed layer. We will see later that our choice of k_0 nearly accounts (perhaps fortuitously) for the low mode baroclinic tidal energy allowed to "radiate" away.

Motivated by microstructure profiles in the abyssal Brazil Basin (St. Laurent et al., 2001) and near the continental slope (Moum et al., 2002), we chose for our vertical structure function a bottom intensified exponential profile of turbulent kinetic energy dissipation with an e-folding scale of 500 m. The vertical structure function $F(z)$ satisfies $\int_{-H}^{0} F(z)\mathrm{d}z = 1$, and is given by

$$F(z) = \frac{\mathrm{e}^{-(H+z)/\zeta}}{\zeta(1-\mathrm{e}^{-H/\zeta})}, \tag{4}$$

where H is the total depth of the water column, and ζ is the vertical decay scale for turbulence.

4. Implementation in an ocean circulation model

In order to determine the long term stability of our parameterization in a global OGCM, it is necessary to run a coarse resolution model that can be integrated for thousands of years. We used Version 3 of the Modular Ocean Model (Pacanowski and Griffies, 1999) on a spherical grid, with a latitudinal resolution of 1.8°, a longitudinal resolution of 3.8°, and 19 vertical levels. The bathymetry is the sub-sampled ETOPO-5 topography and grid used in the University of Victoria climate model (Weaver et al., 2001). In order to maintain stability, the model solution was smoothed by Fourier filtering north of 82° and the northernmost latitude band was converted into land points. In (3) and (4), we take $\zeta = 500$ m, $q = 1/3$, and $k_0 = 0.1$ cm^2 s^{-1}.

In this study, mixing tensor rotation (Griffies et al., 2000) is essential. The Laplacian isopycnal diffusion coefficient was 2×10^7 cm^2 s^{-1} for tracers. No parameterization of mesoscale eddies such as isopycnal thickness diffusion (Gent and McWilliams, 1990; Griffies et al., 1998) was employed. As is commonly done (Large et al., 1994), vertical viscosity was set to be 10 times the vertical diffusion of tracers, although the model was insensitive to our choice of vertical viscosity. Horizontal viscosity was parameterized using a Laplacian diffusion coefficient of 2×10^9 cm^2 s^{-1}. In the deep ocean where stratification is weak, the diffusivity from (3) and (4) was constrained by limiting N^2 to be larger than 10^{-8} s^{-2}. This cutoff only needed to be applied at a few points. The time step was 86,400 s for tracers and 1125 s for velocity. Convection was parameterized by mixing unstable profiles within a single time step to eliminate hydrostatic instability. No bottom boundary layer parameterization was employed, and as is typical for coarse resolution models under such circumstances, northern hemisphere deep water formation occurred convectively south of the Denmark Straits.

The Jayne and St. Laurent (2001) tidal model extends from 72°S to 72°N, whereas our ocean model extends from pole-to-pole. Therefore mixing had to be specified along the Antarctic shelf as

well as in the Arctic. South of 72°S, the model uses background mixing only. In the Arctic, a Peclet number violation occurred (Weaver and Sarachik, 1990), creating spuriously cold water masses. This numerical problem was resolved by setting mixing north of 72°N to a traditional bottom intensified arctangent profile (Bryan and Lewis, 1979) with surface values of 0.3 $cm^2 s^{-1}$ and a transition to 1.3 $cm^2 s^{-1}$ at a depth of about 2500 m. Our fix was not physically motivated and we have not explored its consequences beyond the Arctic. Surface boundary conditions for tracers were obtained by restoring to the World Ocean Atlas (WOA) monthly climatology (Levitus and Boyer, 1994; Levitus et al., 1994b) with time scales of 1/30 days for heat and 1/60 days for salt. The WOA annual mean climatology was also used to initialize the model. Wind stress was taken from the monthly varying Hellerman and Rosenstein (1983) data set. Our philosophy for the design of the experiments was to take an existing ocean model (the oceanic component of the University of Victoria climate model), use standard forcing (relaxation to climatology), and modify only the vertical mixing scheme.

5. Results

All models were run for 4000 years, at which time the trends in globally averaged potential temperature and salinity were less than 0.02 °C and 0.001 psu per thousand years. Model results presented are annual means over the final year of integration. Results are compared with the WOA climatology and with turbulent diffusivity estimates from a variety of sources. In addition, a comparison is made with a control run that has a uniform diffusivity of 0.9 $cm^2 s^{-1}$ specified a postiori from the diagnosed global average vertical mixing in the variable mixing run. In several places we shall also make comparisons to a second control run with an arctangent profile of diffusivity (Bryan and Lewis, 1979) having an upper ocean value of 0.3 $cm^2 s^{-1}$ increasing to 1.3 $cm^2 s^{-1}$ at depth. We will denote the model run with the tidal mixing parameterization the *variable mixing* case, the run with the equivalent uniform mixing to be the *uniform mixing* case, and the run with the arctangent profile to be the *Bryan and Lewis mixing* case. Note that all three cases have the same global average diffusivity of 0.9 $cm^2 s^{-1}$. The variable mixing model is surprisingly stable to a stratification dependent mixing that evolves with the model solution.

5.1. Diffusivity

The globally averaged vertical profile of mixing (Fig. 1) ranges from 0.3 $cm^2 s^{-1}$ in the upper ocean to 7.7 $cm^2 s^{-1}$ at the model's lowest depth level. The ocean global mean value is 0.9 $cm^2 s^{-1}$, remarkably close to the canonical 1 $cm^2 s^{-1}$ estimate (Munk, 1966; Munk and Wunsch, 1998). Note that the global average value at a given level is somewhat misleading. For instance at the $z = 2300$ m level, the global average diffusivity is 0.6 $cm^2 s^{-1}$ (Fig. 2, top panel). However, most of the model domain is close to the background diffusivity of 0.1 $cm^2 s^{-1}$ at this depth. Only a few regions, such as above the mid-Atlantic ridge, contribute to the elevated diffusivity values. Looking at all bottom mixing points (Fig. 2, bottom panel) we see that mixing is greatly elevated, with a mean diffusivity of 2.3 $cm^2 s^{-1}$. This represents an average at a number of depth levels, and thus is different than the global average diffusivity at the lowest depth mixing level (7.7 $cm^2 s^{-1}$).

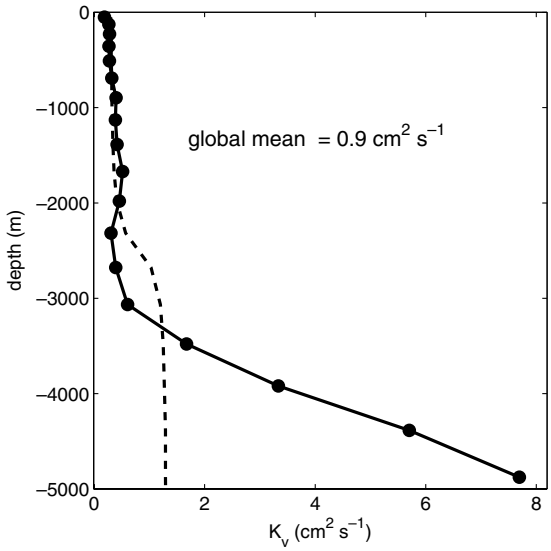

Fig. 1. The average vertical profile of diffusivity for the world ocean. An arctangent diffusivity profile sometimes used in ocean models is shown as the dashed line (Bryan and Lewis, 1979).

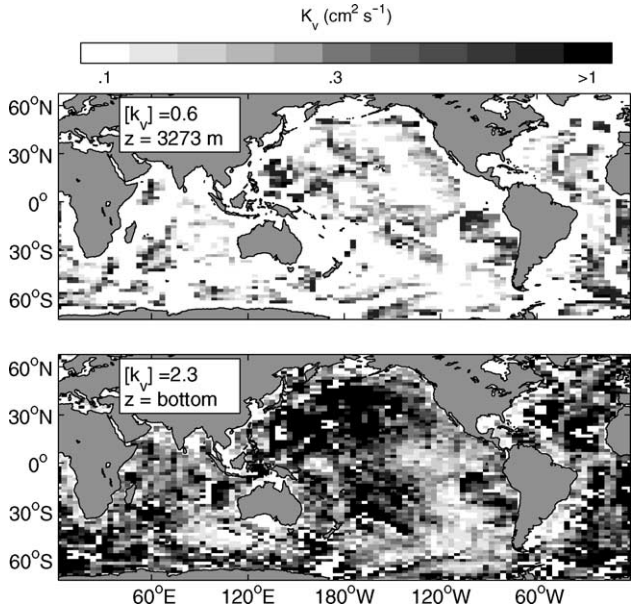

Fig. 2. Upper panel: diffusivity at intermediate depth in the variable mixing model. Lower panel: bottom values of diffusivity. Note that for the lower panel, only 10% of the abyssal ocean has values of k_v greater than 5.0 cm^2 s^{-1}, and more than 50% has values less then 0.25 cm^2 s^{-1}.

Several basin-scale inverse model estimates of diffusivities for the bottom waters of the Pacific, Atlantic, and Indian Oceans have been obtained using sections of temperature and salinity in conjunction with current meter and bio-geochemical data from the World Ocean Circulation

Experiment (see, e.g., Ganachaud and Wunsch, 2000). Defining deep waters as lying between the 27.96 and 28.07 $\mathrm{kg\,m^{-3}}$ neutral surfaces (nominal depth range: 2000–3500 m), Ganachaud and Wunsch found diffusivities of 9 ± 4, 12 ± 7, and 9 ± 2 $\mathrm{cm^2\,s^{-1}}$ for the Atlantic, Indian, and Pacific bottom waters, respectively. For bottom waters in these same basins, we find values of 7.4, 5.4, and 6.5 $\mathrm{cm^2\,s^{-1}}$, agreeing with those of Ganachaud and Wunsch in the Atlantic and Indian Ocean, within their stated error bars. Our diffusivity is somewhat weaker, but of similar magnitude, in the Pacific. In the abyssal Brazil Basin, Morris et al. (2001) estimated a diffusivity of 5.1 ± 3.0 $\mathrm{cm^2\,s^{-1}}$ for waters with potential temperatures colder than 0 °C. In the present study, our corresponding estimate is $k_v = 6.3$ $\mathrm{cm^2\,s^{-1}}$, which is indistinguishable from the Morris et al. estimate. We note that our mixing parameterization accounts for the tidal enhancement of diffusivity only. Other processes such as mixing in hydraulically controlled flows (e.g., Thurnherr et al., 2002) may also contribute to enhanced diffusivities in the real ocean.

5.2. Power consumption

Knowing the diffusivity and the stratification, we can calculate the energy consumption (P) due to vertical mixing by integrating the Osborn (1980) relation, $\epsilon = kN^2\Gamma^{-1}$, over the ocean volume

$$P = \int \rho\epsilon \,\mathrm{d}V = \frac{1}{\Gamma}\int \rho k N^2 \,\mathrm{d}V. \tag{5}$$

In (5) we use k for diffusivity to denote a general relationship between power consumption and diffusivity. Using (5), we can estimate P from (3). A summary of the power consumption due to diapycnal mixing implied by the Osborn relation is given in Table 1. We can separately compute the contribution due to our background diffusivity, k_0 by taking $k = k_0$ in (5). If the ocean model produced a perfect reproduction of the WOA climatology, then the parameterized tidal contribution to mixing would dissipate 0.37 TW in the variable mixing experiment, since our tidal dissipation efficiency, q is 1/3 and the initial energy supplied was 1.10 TW. In the variable mixing case, the final tidal contribution to the steady-state power consumption was 0.36 TW. which differs slightly from the initial input of 0.37 TW since stratification evolves with the ocean model. The background diffusion of 0.1 $\mathrm{cm^2\,s^{-1}}$ contributes another 0.65 TW. The total power consumption due to our vertical mixing scheme (3) is $0.36 + 0.65 = 1.01$ TW in the final state. By contrast, the uniform mixing model ($k_v = 0.9$ $\mathrm{cm^2\,s^{-1}}$) consumes 5.80 TW, and the Bryan and Lewis model consumes 2.11 TW. It is interesting to note the factor of three difference between the energy consumption in the uniform mixing and Bryan and Lewis models, since they have the same global average value of k_v.

Table 1
Summary of power consumption due to diapycnal mixing implied by the Osborn (1980) relation

Experiment	k_0 ($\mathrm{cm^2\,s^{-1}}$)	k_0 contribution (TW)	Tidal contribution (TW)	Total (TW)
Variable	0.1	0.65	0.36	1.01
Uniform	0.9	5.80	N/A	5.80
Bryan and Lewis	0.3–1.3	2.11	N/A	2.11

5.3. Meridional transports

The modeled overturning circulation in the variable mixing case is weaker than that of the uniform mixing case (summarized in Fig. 3 and Table 2). In the Southern Ocean 12.9 Sv (1 Sv = 1×10^6 m^3 s^{-1}) of downwelling occurs in the variable mixing case, and 5.0 Sv are exported into Atlantic. A total of 5.7 Sv are exported into the Pacific and Indian Oceans. In the uniform mixing case, downwelling in the Southern Ocean is 19.0 Sv, with 7.5 Sv entering the Atlantic, and 10.4 Sv entering the combined Pacific and Indian Oceans. Note that in both models, recirculation and water mass modification occurs not only in the Deacon cell (see e.g., Döös and Webb, 1994; Marsh et al., 2000; Speer et al., 2000), but also for dense water formed near the coast of Antarctica. In the latter case, some of this water mixes and resurfaces in the Southern Ocean, and some of it circulates around the Southern Ocean as Circumpolar Deep Water. Thus, the amount of water exported into the various ocean basins is not strictly related to the amount of water downwelling near Antarctica.

In the variable mixing model, 12.8 Sv of North Atlantic Deep Water (NADW) is formed while 22.2 Sv of NADW is formed in the uniform mixing model. In the uniform mixing case, the boundary between NADW and the Antarctic bottom waters is slightly deeper (2100 vs. 2300 m at 18°N). A key difference is that in the overturning for the global circulation in the variable mixing case, we see that the NADW cell extends all the way into the southern hemisphere. This connects with the Deacon cell and hence with upwelling and water mass transformation in the Southern Ocean. In the uniform mixing case NADW upwells in the Southern Ocean as well, but the connection with the Deacon cell is obscured by a strong, shallow overturning cell in the sub-tropical

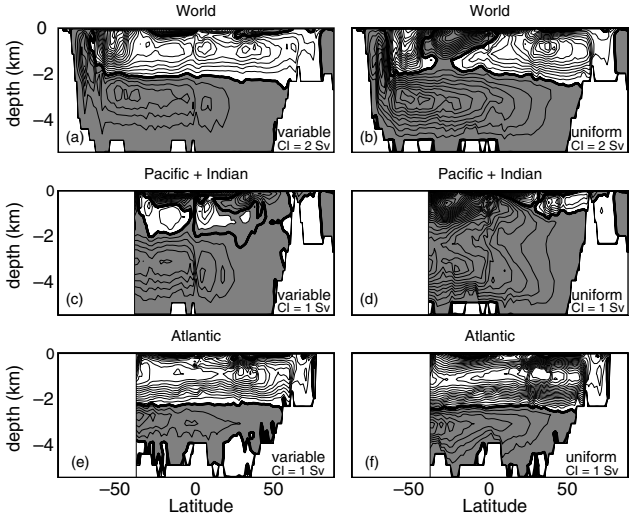

Fig. 3. Meridional overturning streamfunctions for the world ocean (panels (a) and (b), top row), the combined Pacific and Indian Ocean (panels (c) and (d), middle row) and the Atlantic ocean (panels (e) and (f), bottom row). The left column is the variable mixing case, and the right column is the uniform mixing case. For clarity, negative values are shaded and the zero contour is bold. The contour interval is 2 Sv, for the world ocean views (panels (a) and (b)), and 1 Sv for each sub-domain (panels (c)–(f)).

Table 2
Summary of transports discussed in the text

Region	Variable	Uniform
Global Southern Ocean downwelling	−12.9	−19.0
Global abyssal Southern Ocean export	−9.9	−17.8
Abyssal Southern Ocean export into Pacific + Indian Oceans	−5.7	−10.4
North Atlantic downwelling	12.8	22.2
Abyssal Southern Ocean export into abyssal South Atlantic	−5.0	−7.5

The first column indicates the geographic region, and the next two columns give the diagnosed transports based on the extrema in the overturning streamfunction data presented in Fig. 3.

southern Pacific Ocean centered at approximately 600 m depth that is entirely absent in the variable mixing case. The uniform mixing model exports a total of 17.8 Sv out of the Southern Ocean, while the variable mixing model exports 9.9 Sv.

Great differences in overturning arise in the Pacific. In the variable mixing case, most of the flow returns to the Southern Ocean below 2000 m. This is in line with a recent data-based estimate of the overturning in the Pacific showing very little ventilation of the deep water in the North Pacific (Talley et al., submitted for publication). In the uniform mixing case, the inflow is much stronger and better organized, with the abyssal water upwelling all the way to the surface in the North Pacific. Also note the two shallow cells of overturning of positive sign present in the variable mixing case, entirely absent in the uniform mixing model.

The meridional heat transport of the variable mixing model has a very similar structure to data based estimates (Fig. 4). In the southern hemisphere, transport is consistent with inverse estimates (Ganachaud and Wunsch, 2000), with a structure similar to that found by Trenberth and Caron (2001). In contrast, the uniform mixing control run significantly overestimates the data based values in the southern hemisphere. In the northern hemisphere, both the variable and uniform mixing models underestimate the data based curve between 10°N and 40°N. This weak heat transport is typical of low-resolution ocean models. The somewhat larger heat transport in the uniform mixing case is likely due to the unrealistically large mixing in the thermocline. Both models use relaxation boundary conditions. The resulting shortcomings of the modeled heat transports are discussed by Killworth et al. (2000). Note however, the significant difference in heat transport under the same boundary conditions as a result of the two very different mixing parameterizations, even though the volume averaged diffusivity is the same in both experiments.

5.4. Abyssal circulation

Diapycnal upwelling, vertical diffusion, and large-scale circulation are linked through planetary vorticity dynamics. For an abyssal density layer of thickness $h(x,y)$ bounded above by an isopycnal surface $z_i(x,y)$ and below by the ocean bottom, the steady-state inviscid vorticity equation can be written as

$$\beta v - \frac{f}{h}\boldsymbol{u}\cdot\nabla h = \frac{f}{h}w^*(z). \tag{6}$$

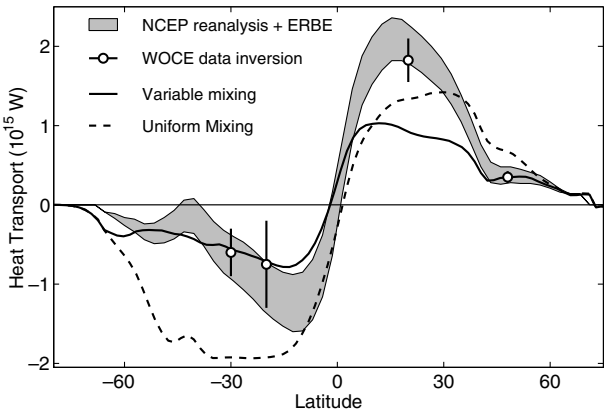

Fig. 4. The meridional heat transport for the global ocean. For comparison, an estimate based on the National Center for Environmental Prediction (NCEP) numerical weather prediction model reanalysis constrained by the Earth Radiation Balance Experiment (ERBE) satellite data (Trenberth and Caron, 2001) is shown (gray band) along with several inverse model estimates (Ganachaud and Wunsch, 2000) derived from World Ocean Circulation Experiment (WOCE) data.

Here, we have used the kinematic definition of the diapycnal mass flux in a steady-state density field,

$$w^* = w - \boldsymbol{u} \cdot \nabla z_i. \tag{7}$$

As discussed by McDougall (1995) and Pedlosky (1996), this is the vertical component of the diapycnal flow. Eq. (6) shows that for a vertical integrated abyssal layer in steady-state, diapycnal mass flux is the vortex stretching that forces meridional flow. Using (7), a steady-state buoyancy budget for the ocean interior can be written as

$$w^* N^2 \cong \frac{\partial}{\partial z}(k_v N^2). \tag{8}$$

Note that lateral advection effects are included in (8) through the definition of w^* in (7). However, in (8) we have neglected buoyancy flux contributions due to cabelling and thermobaricity (McDougall, 1987), as well as another small term for isopycnal curvature that scales as isopycnal slope squared (Garrett, 2001; St. Laurent et al., 2001). This balance links the vertical diapycnal mass flux (w^*) to vertical gradients in the buoyancy flux ($k_v N^2$) and allows us to make a thermodynamic determination of w^*. Through (6), meridional transport is explicitly linked to mixing through the vertical tracer balance.

If we substitute (3) into (8), we obtain

$$w^* = \frac{2k_0}{N}\frac{\partial N}{\partial z} + \frac{\Gamma}{N^2}\frac{\partial \epsilon}{\partial z}. \tag{9}$$

Since stratification generally *decreases* with depth, and our parameterized tidal dissipation, ϵ *increases* with depth, the terms on the right hand side of (9) are of opposite sign. Were there no

uniform background diffusivity, this thermodynamic relation shows that only diapycnal downwelling ($w^* < 0$) would be supported in the interior. However, since the model imposes a no-flux boundary condition along the seafloor, the divergence of buoyancy flux in the model's deepest level always supports diapycnal upwelling ($w^* > 0$). Diapycnal upwelling can also occur in the interior when the term associated with vertical gradient of stratification (first term on the RHS of Eq. (9)) overpowers the term associated vertical gradient of dissipation rate (second term on the RHS of Eq. (9)). In the uniform mixing case, we see that the upwelling is quite uniform over most of the world ocean (Fig. 3), as expected from a consideration of (9) in the absence of a bottom intensified energy source for mixing. It should be noted that it is possible for w and w^* to have opposite signs. For a geometric illustration of this, see Pedlosky (1996, Fig. 3.2.1, p. 101).

In our analysis, we determined w^* kinematically since the information about isopycnal slope is already calculated for the neutral mixing physics modules in the ocean model. Additionally, the thermodynamic calculation of w^* is complicated by the spurious numerical diffusion, arising from the vertical discretization and numerical errors in the model's advection scheme (Griffies et al., 2000). Hence the actual diffusivity influencing the density field of the model is not explicitly known. Thus w^* and the explicit k_v in the model are not necessarily consistent with the vertical tracer balance given by (8).

The global distribution of w^* through 3300 m is shown in Fig. 5. In the variable mixing model (Fig. 5, upper panel), diapycnal upwelling occurs in regions where the mixing is not enhanced above background levels. Additionally, diapycnal upwelling occurs in regions of enhanced dif-

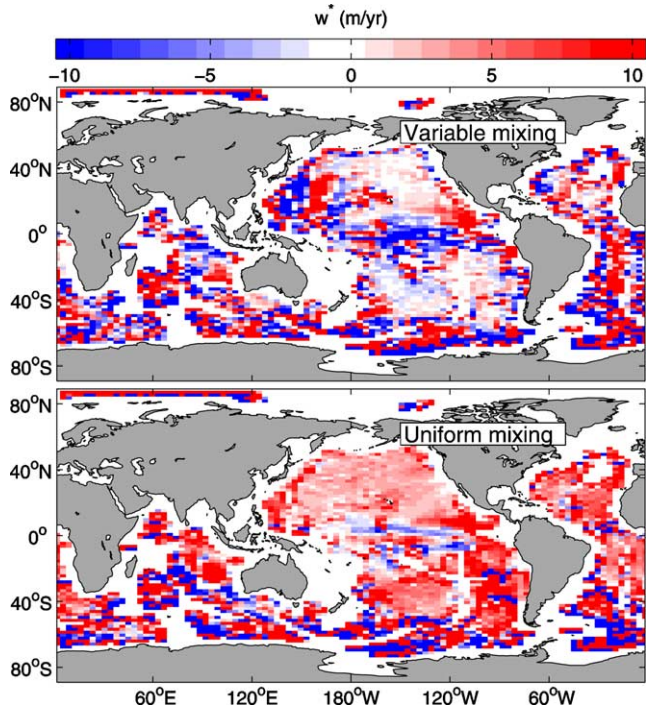

Fig. 5. Diapycnal mass flux (w^*) through the 3300 m depth level.

fusivity, where the 3300 m depth level bounds the deepest layer of the model. Diapycnal downwelling occurs in regions where the diffusivity is enhanced outside of the bottom layer. In the uniform mixing model (Fig. 5, lower panel), and in the model using the Bryan and Lewis diffusivity profile (not shown), diapycnal downwelling occurs over a much smaller area.

We have also examined the abyssal circulation predicted by our model runs. Examining subthermocline flow along isopycnals in the North Pacific, we find large differences between the spatially variable and uniform mixing experiments (Fig. 6). The along-isopycnal flow in the variable mixing case is much more spatially inhomogeneous and convoluted. Notice e.g., the opposite flow direction along 18°S. Fig. (7) shows deep flow in the abyssal Brazil and Angola Basins. In the variable mixing case, the northward flow of Antarctic bottom water in the Brazil Basin is stronger than in the uniform case. This might seem strange in light of the fact that the net meridional mass transport into the Atlantic is weaker in the variable mixing case (Fig. 3), but note that a considerable portion of this flow directed through the model's Romanche gap and into the Angola Basin where it recirculates to the south. In the variable mixing model the flow through the Romanche gap into the Angola Basin is 0.8 Sv, roughly consistent with current meter observations (Mercier and Speer, 1998). In contrast, the uniform mixing model's flow is directed from the Angola Basin into the Brazil Basin. We note that both models fail to reproduce some aspects of the observed abyssal circulation. For example, the flow along the flanks of the MAR is strongly influenced by blocking from small-scale topography (Thurnherr and Speer, submitted for publication) unresolved by our coarse model. This effect is not resolved in our coarse resolution model.

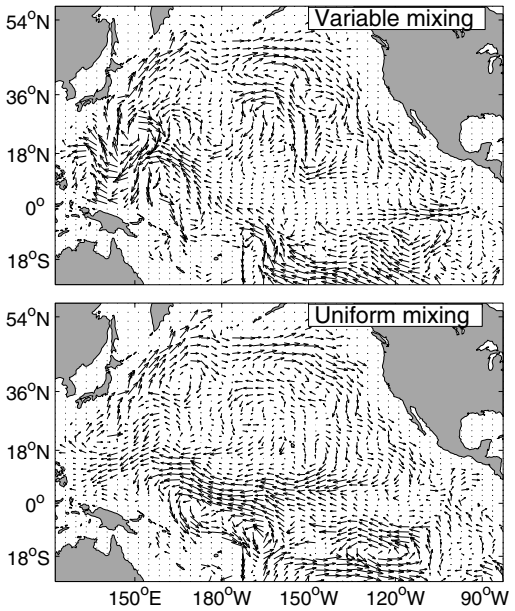

Fig. 6. Vertically averaged isopycnal flow below the $\sigma_2 = 37$ surface (at a nominal depth of 3300 m) in the North Pacific.

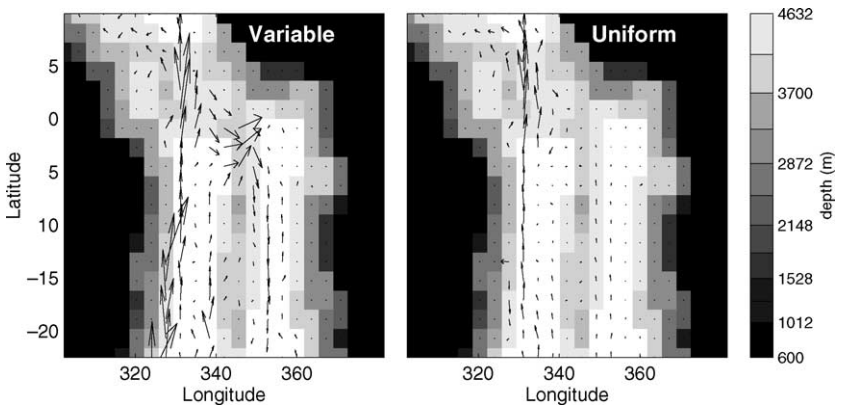

Fig. 7. Vertically averaged flow below the $\sigma_2 = 37.2\ \mathrm{kg\,m^{-1}}$ surface (at a nominal depth of roughly 3300 m) in the abyssal Brazil and Angola Basins. The mid-Atlantic ridge (MAR) is the meridional feature running through the center of each basin. The abyssal Brazil and Angola Basins are the sub-basins to the west and east of the MAR respectively, and the modeled Romanche Gap occurs in the region where there is eastward flow in the variable mixing model.

5.5. Water masses

We have examined the deep temperature and salinity fields resulting from the uniform, variable, and Bryan and Lewis mixing schemes. These results are summarized in Fig. 8. Relative to the WOA climatology (Levitus and Boyer, 1994; Levitus et al., 1994a), the variable mixing model has

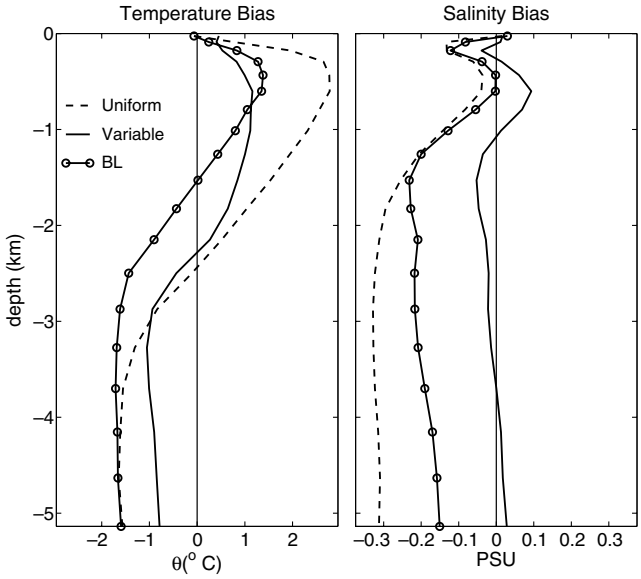

Fig. 8. Globally averaged temperature bias (left panel) and salinity bias (right panel) measured as a departure from climatology (Levitus and Boyer, 1994; Levitus et al., 1994a). Results from models using the uniform, variable, and Bryan and Lewis (BL) mixing schemes are shown.

the smallest bias. The root-mean-square temperature bias in the variable mixing case is 0.9 °C, while the uniform mixing model's bias is a factor of 2 larger. The respective salinity biases are 0.04 and 0.32 psu. Note that the improvement occurs in the upper ocean as well as the deep ocean. Based on this simple metric, the Bryan and Lewis mixing profile does present advantages over the uniform mixing profile, but still has significantly larger biases than the variable mixing model. These results point to the deleterious effects of using unrealistically large diffusivities in the upper ocean and to the benefits of spatially variable diffusion.

6. Discussion

Energy flux out of the barotropic tides into baroclinic waves in the deep ocean has been estimated by a tidal model to be 1.10 TW (Jayne and St. Laurent, 2001), in quantitative agreement with observationally based estimates (Egbert and Ray, 2000, 2001). Turbulent dissipation was then inferred assuming that 1/3 of this energy flux dissipates locally. This dissipation is modeled as a depth dependent profile that decreases exponentially with height above the bottom. An attractive feature of this parameterization is that the mixing evolves spatially and temporally as part of the model solution. The mixing parameterization implicitly includes information about the spatial structure of baroclinic tidal energy and the sub-grid scale roughness of the sea floor.

The power consumption in the variable mixing case remained quite close to that estimated by the tidal model, with only a weak drift due to the changing stratification. We chose a tidal dissipation efficiency of 1/3. The total power consumption in the final state was 1.01 TW, with 0.65 TW attributed to the background mixing, $k_0 = 0.1$ cm^2 s^{-1}. While interesting, the fact that the power consumption by k_0 alone very nearly equals the $1 - q = 2/3$ of the energy "unused" in our parameterization must be regarded as fortuitous. Thus, we have not strictly closed the baroclinic tidal budget in this model. If the goal were to account for additional energy sources, adding up to the 2 TW estimated by Munk and Wunsch (1998), then additional mixing would need to specified.

The new mixing scheme produces notable improvements in the representation of water masses. The root-mean-square temperature bias, relative to a climatology, is reduced by a factor of 2, and the salinity bias is reduced by a factor of 8. A globally averaged diffusivity of 0.9 cm^2 s^{-1} is in close agreement with independent global scale budgets (Munk, 1966; Munk and Wunsch, 1998). We note that the globally averaged profile has certain similarities to the arctangent mixing profile sometimes used in ocean models (Bryan and Lewis, 1979), although the abyssal values are higher in the variable mixing case. The globally averaged variable mixing profile (Fig. 1) is the result of averaging many profiles which individually have nearly uniform weak mixing throughout the water column and larger mixing occurring within a 500 m e-folding scale above the bottom. Also, mixing is only intensified above rough topography and only in regions of baroclinic tide generation. As illustrated in Fig. 2, and corroborated by observations, there are many regions of the ocean where only weak mixing is occurring throughout the water column.

We found that integral transport properties such as the meridional transport of heat and mass are similar in the Bryan and Lewis and variable mixing cases. However, these are significantly different from the uniform mixing case. It appears that the zonally averaged meridional transport properties of the model are largely controlled by the average vertical profile of diffusion. However, the improved temperature and salinity in the variable mixing experiment suggests that water mass

transformations essential to establishing global scale thermohaline structure are a result of local variations in diffusivities. These cannot be captured by any single globally averaged profile for mixing.

We can speculate about the applicability of our parameterization to the ocean component of paleoclimate models. Because more than half of the 3.5 TW known to be dissipated by the ocean tides occurs on continental shelves, large changes in sea level would very likely result in a larger portion of the tidal energy dissipation occurring in the deep ocean. Our parameterization would predict enhanced deep mixing under such circumstances. While it may be reasonable to use our tidal sub-model data to estimate energy flux and diapycnal mixing, one should only do so for configurations which have a modern distribution of continents, continental shelves, and sea-level. This recommendation is made noting that as a practical matter, our parameterization does not directly make use of the energy flux computed by the tidal model, but rather recomputes the flux using the sub-grid scale roughness and barotropic tidal currents and the ocean's modeled stratification. We found that the barotropic tidal currents depend only weakly on the abyssal stratification in the tidal model, although this has not yet been investigated carefully.

The current generation of ocean models have undergone meticulous tuning based on several decades of experience with fixed mixing rates. We deliberately chose to avoid such tuning exercises. There is little doubt that further improvements could be realized with our scheme as a result of subsequent tuning, with important consequences for modeling the oceanic general circulation. Considering the limitations of our ocean-only coarse resolution model and the crudeness of our surface forcing, the variable mixing model's performance is encouraging. We feel that there are obvious steps for further exploring the usefulness of our mixing parameterization. These include increasing horizontal and vertical resolution and coupling to an atmospheric model. Moreover, further refinement of the mixing parameterization should be explored. Improved estimates of baroclinic tidal energy are clearly possible, perhaps through refinements to parameterizations in Laplace tidal equation models (Arbic and Garner, 2002). Additionally, theoretical studies could provide the basis for specifying the depth dependent profile of turbulent dissipation (Polzin, 1999). To fully parameterize mixing in an OGCM, all sources of mixing must be considered. These include turbulent entrainment in regions of dense overflows, turbulence in the oceanic mixed layer, wind generation of inertial waves, and lee wave generation by non-tidally driven flows.

Acknowledgements

We thank A. Thurnherr, R.X. Huang, J. Toole, S. Griffies, B. Arbic, and an anonymous reviewer for helpful comments. This research was supported by an NSF International Research Fellowship to HLS and operating grants from NSERC, the Canadian Institute for Climate Studies/Meteorological Research Service of Canada, the International Arctic Research Center, NOAA's Geophysical Fluid Dynamics Laboratory, and the Arctic Regional Supercomputer Center. SRJ was supported by NASA through JPL contract 1234336 to WHOI and NSF grant ATM-0200929. LCS was supported by the Natural Science and Engineering Research Council of Canada and the US Office of Naval Research. This is Woods Hole Oceanographic Contribution Number 10735.

References

Alford, M.H., 2001. Internal swell generation: the spatial distribution of energy flux from the wind to mixed layer near-inertial motions. J. Phys. Oceanogr. 31, 2359–2368.

Arbic, B.K., Garner, S.T., 2002. A parameterization for abyssal tidal dissipation based on non-radiating drag. EOS Trans. Am. Geophys. Union 83 (4), Ocean Sciences Meet. Suppl., Abstract OS51D-09.

Barton, E.D., Hill, A.E., 1989. Abyssal flow through the Amirante Trench (Western Indian Ocean). Deep-Sea Res. 36, 1121–1126.

Bryan, F., 1987. Parameter sensitivity of primitive equation ocean general circulation models. J. Phys. Oceanogr. 17, 970–985.

Bryan, K., Lewis, L., 1979. A water mass model of the world ocean. J. Geophys. Res. 84, 2503–2517.

Cummins, P.F., Holloway, G., Gargett, A., 1990. Sensitivity of the GFDL ocean general circulation model to a parameterization of vertical diffusion. J. Phys. Oceanogr. 20, 817–830.

Döös, K., Webb, D.J., 1994. The Deacon cell and other meridional cells of the Southern Ocean. J. Phys. Oceanogr. 24, 429–442.

Egbert, G.B., Ray, R.D., 2000. Significant dissipation of tidal energy in the deep ocean inferred from satellite altimeter data. Nature 405, 775–778.

Egbert, G.B., Ray, R.D., 2001. Estimates of M_2 tidal energy dissipation from TOPEX/POSEIDON altimeter data. J. Geophys. Res. 106, 22475–22502.

Ferron, B., Mercier, H., Speer, K., Gargett, A., Polzin, K., 1998. Mixing in the Romanche fracture zone. J. Phys. Oceanogr. 28, 1929–1945.

Ganachaud, A., Wunsch, C., 2000. Improved estimates of global ocean circulation, heat transport and mixing from hydrographic data. Nature 408, 453–457.

Gargett, A.E., 1984. Vertical eddy diffusivity in the ocean interior. J. Mar. Res. 46, 359–493.

Garrett, C., 2001. An isopycnal view of near-boundary mixing. J. Phys. Oceanogr. 31, 138–142.

Gent, P.R., McWilliams, J.C., 1990. Isopycnal mixing in ocean circulation models. J. Phys. Oceanogr. 20, 150–155.

Griffies, S., Pacanowski, R., Hallberg, R., 2000. Spurious diapycnal mixing associated with advection in a *z*-coordinate ocean model. Mon. Weather Rev. 128, 538–564.

Griffies, S.M., Gnanadesikan, A., Pacanowski, R., Larichev, V., Dukowicz, J., Smith, R., 1998. Isoneutral diffusion in a *z*-coordinate ocean model. J. Phys. Oceanogr. 28, 805–830.

Hasumi, H., Suginohara, N., 1999. Effects of locally enhanced vertical diffusivity over rough bathymetry on the world ocean circulation. J. Geophys. Res. 104, 23367–23374.

Hellerman, S., Rosenstein, M., 1983. Normal monthly wind stress over the world ocean with error estimates. J. Phys. Oceanogr. 13, 1093–1104.

Heywood, K.J., Naviera Garabato, A.C., Stevens, D.P., 2002. High mixing rates in the abyssal Southern Ocean. Nature 415, 1011–1014.

Hogg, N., Biscaye, B., Gradner, E., Schmitz, W.J., 1982. On the transport of Antarctic bottom water in the Vema Channel. J. Mar. Res. 40, 231–262.

Huang, R.X., 1999. Mixing and energetics of the oceanic thermohaline circulation. J. Phys. Oceanogr. 29, 727–746.

Huang, R.X., Xiangze, J., 2002. Deep circulation in the South Atlantic induced by bottom-intensified mixing over the mid-ocean ridge. J. Phys. Oceanogr. 32, 1150–1164.

Jayne, S.R., St. Laurent, L.C., 2001. Parameterizing tidal disspiation over rough topography. Geophys. Res. Lett. 28, 811–814.

Killworth, P.D., Smeed, D.A., Nurser, A.J.G., 2000. The effects on ocean models of relaxation toward observations at the surface. J. Phys. Oceanogr. 30, 160–174.

Kunze, E., Toole, J.M., 1997. Tidally driven vorticity, diurnal shear, and turbulence atop Fieberling Seamount. J. Phys. Oceanogr. 27, 2663–2693.

Kunze, E., Rosenfeld, L.K., Carter, G.S., Gregg, M.C., 2002. Internal waves in Monterey Submarine Canyon. J. Phys. Oceanogr. 32, 1890–1913.

Large, W.G., McWilliams, J.C., Doney, S.C., 1994. Oceanic vertical mixing: a review and a model with a nonlocal boundary layer parameterization. Rev. Geophys. 32, 363–403.

Ledwell, J.R., Watson, A.J., Law, C.S., 1993. Evidence for slow mixing across the pycnocline from an open-ocean tracer-release experiment. Nature 364, 701–703.
Ledwell, J.R., Watson, A.J., Law, C.S., 1998. Mixing of a tracer released in the pycnocline. J. Geophys. Res. 103, 21499–21529.
Ledwell, J.R., Montgomery, E.T., Polzin, K.L., Laurent, L.C.S., Schmitt, R.W., Toole, J.M., 2000. Mixing over rough topography in the Brazil Basin. Nature 403, 179–182.
Levitus, S., Boyer, T.P., 1994. NOAA Atlas NESDIS 4, World Ocean Atlas 1994, Temperature, vol. 4. NOAA, US Dept. Commerce, 117 pp.
Levitus, S., Antonov, J.I., Boyer, T.P., 1994a. Interannual variability of temperature at a depth of 125 meters in the North Atlantic Ocean. Science 266, 96–99.
Levitus, S., Burgett, R., Boyer, T.P., 1994b. NOAA Atlas NESDIS 3, World Ocean Atlas 1994, Salinity, vol. 3. NOAA, U.S. Dept. Commerce, 99 pp.
Lien, R.-C., Gregg, M.C., 2001. Observations of turbulence in a tidal beam and across a coastal ridge. J. Geophys. Res. 106, 4575–4591.
Lueck, R.G., Mudge, T.D., 1997. Topographically induced mixing around a shallow seamount. Science 276, 1831–1833.
Marotzke, J., 1997. Boundary mixing and the dynamics of three-dimensional thermohaline circulation. J. Phys. Oceanogr. 27, 1713–1728.
Marsh, R., Nurser, A.J., Megann, A.P., New, A.L., 2000. Water mass transformation in the Southern Ocean of a global isopycnal coordinate GCM. J. Phys. Oceanogr. 30, 1013–1045.
McDougall, T.J., 1987. Thermobaricity, cabelling, and water mass conversion. J. Geophys. Res. 92, 5448–5464.
McDougall, T.J., 1995. The influence of ocean mixing on the absolute velocity vector. J. Phys. Oceanogr. 25, 705–725.
Mercier, H., Speer, K., 1998. Transport of bottom water in the Romanche fracture zone and the chain fracture zone. J. Phys. Oceanogr. 28, 779–790.
Morris, M., Hall, M.H., Laurent, L.C.S., Hogg, N.G., 2001. Abyssal mixing in the Brazil Basin. J. Phys. Oceanogr. 31, 3331–3348.
Moum, J.N., Caldwell, D.R., Nash, J.D., Gunderson, G.D., 2002. Observations of boundary mixing over the continental slope. J. Phys. Oceanogr. 32, 2113–2130.
Munk, W., 1966. Abyssal recipes. Deep Sea Res. 13, 707–730.
Munk, W., 1981. Internal waves and small-scale processes. In: Warren, B.A., Wunsch, C. (Eds.), Evolution of Physical Oceanography—Scientific Surveys in Honor of Henry Stommel. MIT Press, pp. 264–291.
Munk, W.H., Wunsch, C., 1998. Abyssal recipes II: energetics of tidal and wind mixing. Deep Sea Res. 45, 1977–2010.
Niwa, Y., Hibiya, T., 2001. Numerical study of the spatial distribution of the M_2 internal tide in the Pacific Ocean. J. Geophys. Res. 106, 22229–22441.
Osborn, T.R., 1980. Estimates of the local rate of vertical diffusion from dissipation measurements. J. Phys. Oceanogr. 10, 83–89.
Pacanowski, R., Griffies, S., 1999. MOM 3 Manual, GFDL Ocean Group Technical Report. NOAA, GFDL, Princeton, 658 pp.
Pacanowski, R.C., Philander, S.G.H., 1981. Parameterization of vertical mixing in numerical models of tropical oceans. J. Phys. Oceangr. 11, 1443–1451.
Pedlosky, J., 1996. Ocean Circulation Theory. Springer, pp. 453.
Pinkel, R., Munk, W., Worcester, P., et al., 2001. Ocean mixing studied near the Hawaiian Ridge. EOS Trans. Am. Geophys. Union 81, 545 and 553.
Polzin, K., 1999. A rough recipe for the energy balance of quasi-steady internal lee waves. In: Müller, P., Henderson, D. (Eds.), Dynamics of Oceanic Internal Gravity Waves II, Proceedings of the 'Aha Huliko'a Hawaiian Winter Workshop University of Hawaii at Manoa, January 1999. University of Hawaii, School of Ocean and Earth Science and Technology Special Publication, pp. 117–128.
Polzin, K.L., Toole, J.M., Ledwell, J.R., Schmitt, R.W., 1997. Spatial variability of turbulent mixing in the abyssal ocean. Science 276, 93–96.
Roemmich, D., Hautala, S., Rudnick, D., 1996. Northward abyssal transport through the Samoan passage and adjacent regions. J. Geophys. Res. 101, 14039–14056.

Saunders, P.M., 1987. Flow though discovery gap. J. Phys. Oceanogr. 17, 631–643.
Sokolov, A., Wang, C., Holian, G., Stone, P., Prinn, R., 1998. Uncertainty in the ocean heat and carbon uptake and its impact on climate projections. Geophys. Res. Lett. 25, 3603–3606.
Speer, K., Rintoul, S.R., Sloyan, B., 2000. The diabatic Deacon cell. J. Phys. Oceanogr. 30, 3212–3222.
St. Laurent, L.C., Garrett, C., 2002. The role of internal tides in mixing the deep ocean. J. Phys. Oceanogr. 32, 2882–2899.
St. Laurent, L.C., Toole, J.M., Schmitt, R.W., 2001. Bouyancy forcing by turbulence above rough topography in the abyssal Brazil Basin. J. Phys. Oceanogr. 31, 3476–3495.
St. Laurent, L.C., Simmons, H.L., Jayne, S.R., 2002. Estimating tidally driven mixing in the deep ocean. Geophys. Res. Lett. 29, 2106, 10.1029/2002GL015 633.
Talley, L.D., Reid, J.L., Robbins, P.E. Data-based meridional overturning streamfunctions for the global ocean. J. Climate, submitted for publication.
Thurnherr, A.M., Speer, K.G. Boundary mixing and topographic blocking on the mid-Atlantic ridge in the South Atlantic. J. Phys. Oceanogr., 33 (4), 848–862.
Thurnherr, A.M., Richards, K.J., German, C.R., Lane-Serff, G.F., Speer, K.G., 2002. Flow and mixing in the rift valley of the mid-Atlantic ridge. J. Phys. Oceanogr. 32, 1763–1778.
Trenberth, K.E., Caron, J.M., 2001. Estimates of meridional atmospheric and ocean heat transports. J. Climate 14, 3343–3443.
Watanabe, M., Hibiya, T., 2002. Global estimates of the wind-induced energy flux to inertial motions in the surface mixed layer. Geophys. Res. Lett. 29, 1239, 10.1029/2001GL014 422.
Weaver, A. et al., 2001. The UVic earth system climate model: model description, climatology and application to past, present and future climates. Atmos.-Ocean 39, 361–428.
Weaver, A.J., Sarachik, E.S., 1990. On the importance of vertical resolution in certain ocean general circulation models. J. Phys. Oceanogr. 20, 600–609.
Webb, D.J., Suginohara, N., 2001. The interior circulation of the ocean. In: Siedler, G., Church, J., Gould, J. (Eds.), Ocean Circulation and Climate. In: International Geophysics Series, vol. 77. Academic Press, pp. 205–214.
Whitehead, J.A., Worthington, L.V., 1982. The flux and mixing rates of Antarctic bottom water within the North Atlantic. J. Geophys. Res. 101, 7903–7924.
Wunsch, C., 1998. The work done by the wind on the ocean circulation. J. Phys. Oceanogr. 28, 2332–2340.
Zhang, J., Schmitt, R.W., Huang, R.X., 1999. The relative influence of diapycnal mixing and hydrologic forcing on the stability of the thermohaline circulation. J. Phys. Oceanogr. 29, 1096–1108.